Mon. Not. R. Astron. Soc. **399,** 385–398 (2009) doi:10.1111/j.1365-2966.2009.15286.x

The history of the Solar system's debris disc: observable properties of the Kuiper belt

Mark Booth,[1⋆] Mark C. Wyatt,[1] Alessandro Morbidelli,[2] Amaya Moro-Martín[3,4] and Harold F. Levison[5]

[1]*Institute of Astronomy, Madingley Rd, Cambridge CB3 0HA*
[2]*Observatoire de la Côte d'Azur, Nice, France*
[3]*Centro de Astrobiologia - CSIC/INTA, 28850 Torrejón de Ardoz, Madrid, Spain*
[4]*Department of Astrophysical Sciences, Peyton Hall, Ivy Lane, Princeton University, Princeton, NJ 08544, USA*
[5]*Department of Space Studies, Southwest Research Institute, Boulder, CO 80302, USA*

Accepted 2009 June 18. Received 2009 June 16; in original form 2009 April 28

ABSTRACT

The Nice model of Gomes et al. suggests that the migration of the giant planets caused a planetesimal clearing event, which led to the late heavy bombardment (LHB) at 880 Myr. Here, we investigate the infrared emission from the Kuiper belt during the history of the Solar system as described by the Nice model. We describe a method for easily converting the results of *N*-body planetesimal simulations into observational properties (assuming blackbody grains and a single size distribution) and further modify this method to improve its realism (using realistic grain properties and a three-phase size distribution). We compare our results with observed debris discs and evaluate the plausibility of detecting an LHB-like process in extrasolar systems. Recent surveys have shown that 4 per cent of stars exhibit 24 μm excess and 16 per cent exhibit 70 μm excess. We show that the Solar system would have been amongst the brightest of these systems before the LHB at both 24 and 70 μm. We find a significant increase in 24 μm emission during the LHB, which rapidly drops off and becomes undetectable within 30 Myr, whereas the 70 μm emission remains detectable until 360 Myr after the LHB. Comparison with the statistics of debris disc evolution shows that such depletion events must be rare occurring around less than 12 per cent of Sun-like stars and with this level of incidence we would expect approximately one of the 413 Sun-like field stars so far detected to have a 24 μm excess to be currently going through an LHB. We also find that collisional processes are important in the Solar system before the LHB and that parameters for weak Kuiper belt objects are inconsistent with the Nice model interpretation of the LHB.

Key words: Kuiper Belt – Solar system: general – circumstellar matter – planetary systems.

1 INTRODUCTION

Over the past couple of decades, an increasing number of stars have been found to be orbited by discs of planetesimals and dust known as debris discs. As more and more discs are discovered, it becomes possible to start building up a picture of how these debris discs evolve over time (see Wyatt 2008, for a review). Recent surveys (e.g. Hillenbrand et al. 2008; Trilling et al. 2008; Carpenter et al. 2009) have shown that the number of Sun-like stars that have been observed with 24 μm emission (produced by hot dust) decreases with age, but the number of stars with 70 μm emission (produced by cold dust) remains approximately constant with age. These observations generally agree with models suggesting that debris discs evolve in steady state becoming collisionally depleted over time (Löhne, Krivov & Rodmann 2008), although there are a few exceptions that have much more hot dust than would be expected from these collisional arguments (Wyatt et al. 2007a).

The Solar system has its own debris disc, with the majority of its mass concentrated in the asteroid belt and Kuiper belt. These belts correspond to the hot dust and cold dust seen around other stars, but our own disc is much less massive than these observed discs (Moro-Martín et al. 2008). Simulations of accretion in the Kuiper belt and the formation of binary Kuiper belt objects (KBOs) suggest that the original Kuiper belt must have been much more massive for the largest objects to form (e.g. Stern 1996a; Chiang et al. 2007), which leads to the 'missing mass problem' of the Kuiper belt as this mass deficit cannot be explained by collisional processes alone.

⋆E-mail: mbooth@ast.cam.ac.uk

One model that does explain the missing mass of the Kuiper belt – along with the orbits of the giant planets and various other details of the structure of the Solar system – is the Nice model (Gomes et al. 2005; Morbidelli et al. 2005; Tsiganis et al. 2005; Levison et al. 2008a). The Nice model was designed to explain the current orbital elements of the outermost planets (Tsiganis et al. 2005). It is based on the idea that the gas giants formed much closer together. Due to interactions with the planetesimal disc, Saturn, Neptune and Uranus migrated outwards and Jupiter migrated slightly inwards. When Jupiter and Saturn crossed their 2:1 mean motion resonance (MMR), the system became temporarily destabilized, affecting the orbital elements of the gas giants. As Neptune moved out into the Kuiper belt, it dynamically excited the orbits of many of the KBOs, causing them to evolve on to cometary orbits and impact the terrestrial planets and moons. As the planets' orbits evolved, secular resonance sweeping would have excited the orbits of many of the asteroids (Gomes 1997), thus also causing a bombardment of asteroids on the planets and moons of the inner Solar system. Hence, the Nice model also explains the late heavy bombardment (LHB) of the Moon – a period of intense bombardment in which most of the craters on the Moon were formed, which occurred around 3.9 billion years ago (Tera, Papanastassiou & Wasserburg 1974), of which the latest impactors were most likely main belt asteroids (Kring & Cohen 2002; Strom et al. 2005).

This period of intense bombardment and dynamical depletion of the Kuiper belt is likely to have had a significant effect on the observable properties of the debris disc of the Solar system. In this paper, we investigate this effect by converting the distributions of planetesimal mass from the Nice model into distributions of emitting surface area to discover how the Solar system would have appeared to a distant observer during its history. Although the Solar system's debris disc has a number of components, for this paper we concentrate on the changes to the Kuiper belt and how this would have affected the observable properties of the Solar system. In Section 2, we describe the Nice model data and the simple analytical model applied to it, which uses the assumption of blackbody grains and a single-slope size distribution. In Section 3, we look into relaxing the assumptions of blackbody emission and a single-slope size distribution to discover how a more realistic model changes our initial conclusions. Our final conclusions are given in Section 4.

2 MODELLING

2.1 The Nice model data

Our model is based on planetesimal data from one of the Nice model runs (Gomes et al. 2005). In the Nice model, the simulation begins with effectively 10 000 particles, each representing 1.05×10^{-8} $M_\odot$ of KBOs. Any particles that reached a heliocentric distance of 1000 au or evolved on to orbits with perihelion, $q < 1$ au were removed from the simulation. The data cover a 1.2 Gyr time period starting at the time at which the gas disc dissipates. Gomes et al. (2005) ran eight simulations with varying disc inner radius. The data used here are for the run with a disc inner edge of ∼15.5 au, which places the LHB at 879 Myr, close to the ∼700 Myr given by the analysis of Strom et al. (2005). This is also the most realistic of the Gomes et al. (2005) runs since particles within ∼15.3 au have dynamical lifetimes shorter than the gas disc lifetime showing that they would have disappeared by the time the gas disc dissipates. This run starts with an initial disc mass of 35 $M_\oplus$ and has 24 $M_\oplus$ at the time of the LHB. If the disc is less massive than this, Jupiter and Saturn do not cross their 2:1 MMR and there is no LHB. If the disc is more massive, then the final separation of Jupiter and Saturn is much larger than it is today.

2.2 Mass evolution

Using the orbital elements of the Nice model particles, we can then calculate the position of the particles at each time-step. For now, it is the one-dimensional distribution that we are interested in and so the particles are separated into radius bins to allow us to determine the mass distribution in the system. Due to the small number of particles in the simulation, the evolution of the mass distribution appears stochastic in each 1 Myr time-step. To smooth out the evolution and make it more realistic, two changes are made. First, each particle is replaced by 10 particles, each of which is one-tenth of the original mass, and these particles are spread uniformly around the orbit in mean anomaly to simulate the entire range of radii that particle would have passed through during this time period. By doing this, we lose any resonant structures present in the data but increase the resolution of the model. Secondly, the mass distribution at each time-step is averaged over five time-steps (∼5 Myr). Thus, any values given in this paper at a specific time are actually averaged over 5 Myr.

Fig. 1 shows the surface density of the disc: just before the LHB (at 873 Myr), during the LHB (at 881 Myr) and at the end of the simulation (at 1212 Myr). Henceforth, we refer to these epochs as pre-LHB, mid-LHB and post-LHB. Before the LHB occurs, most of the planetesimals are confined to a ring ∼15 au wide, centred at about 26 au. The surface density profile interior to this ring (over the range 8–19 au) has a slope of $R^{2.9\pm0.4}$ and outside the ring (over the range 38–106 au) the slope is $R^{-3.2\pm0.2}$. The mass surface density within the ring is 2 orders of magnitude above this. At the onset of the LHB, a large number of the planetesimals are scattered from the belt both inwards and outwards spreading out the distribution of mass. Although planetesimals are scattered inwards before the LHB, at the onset of the LHB the rate at which planetesimals are being scattered inwards is much greater than the rate at which they are scattered back out. This results in a surface density profile with a leading slope of $R^{1.5\pm0.1}$ between 1 and 27 au and a trailing slope of $R^{-4.8\pm0.1}$ between 27 and 106 au at 881 Myr. By 1212 Myr, the planetesimals are highly scattered giving a surface density profile with a leading slope (over the range 9–38 au) of $R^{3.4\pm0.4}$ and a trailing slope (over the range 38–106 au) of $R^{-2.7\pm0.1}$.

Levison et al. (2006) ran simulations of ecliptic comets to help them understand the orbit of the comet 2P/Encke. Their data can

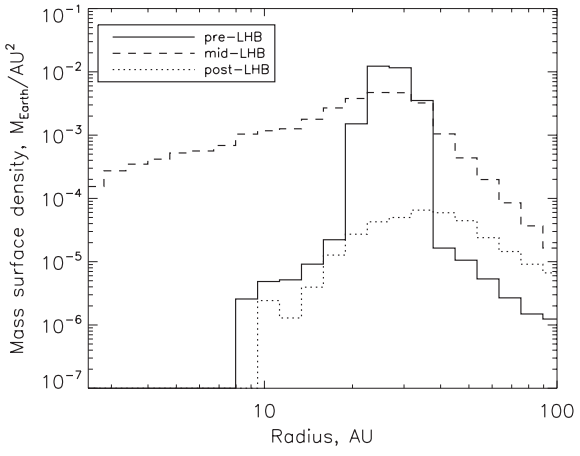

Figure 1. Mass distribution before, during and after the LHB.

be used to find the spatial distribution of comets, which we might expect to be similar to our distribution at the end of the Nice model. Between 9 and 38 au, the number density of comets is proportional to $R^{2.7}$ and between 38 and 106 au the number density is proportional to $R^{-2.5}$. Our slope for the inner region is steeper than that found by Levison et al. (2006) and there are no particles within 9 au whereas their comet model includes particles as far in as 0.1 au. In part, this difference is because the Nice model removes particles as soon as $q < 1$ au therefore underestimating the number of comets in this region. The slopes for the outer region compare much better despite the fact that Levison et al. (2006) only include objects that have interacted with Neptune in their simulations suggesting that cometary dynamics is broadly similar, at least in terms of spatial distribution.

The Nice model ends roughly 3 Gyr ago. For this work, we would like to extrapolate the post-LHB evolution so that we can compare the predictions of the Nice model with current observations of the Solar system and compare our model with observations of extrasolar debris discs. To do this, we need to find how the mass of the system will continue to evolve after the end of the LHB.

At the end of the Nice model run, there are 322 particles remaining. Many of these particles have left the confines of the Kuiper belt, becoming comets and scattered disc objects (SDOs), with only a few remaining as classical Kuiper belt objects (CKBOs). Here, we define CKBOs as objects with $q > 38$ au and $42 < a < 47$ au and assume that, since these objects are now on orbits that no longer bring them close to Neptune (or any of the other planets), they would be expected to remain trapped in the classical belt for the rest of the Solar system's lifetime (Levison et al. 2008a). In reality, the mass of the CKB will be decreased due to chaotic diffusion by resonances, small KBOs encountering large KBOs and collisions. However, this reduction in mass is a small fraction of the total mass (Gomes et al. 2008). From this definition, we find that three out of the 322 particles represent CKBOs and that the mass of the classical Kuiper belt remains fixed at $M_{\rm CKB} = 0.010 \pm 0.006\ {\rm M}_\oplus$, which compares favourably with recent observational estimates – 0.008–0.1 $\rm M_\oplus$ (Gladman et al. 2001; Bernstein et al. 2004; Fuentes & Holman 2008) – although this may be an underestimate as the more detailed modelling of Levison et al. (2008a), which includes dynamical processes not present in Gomes et al. (2005), gives a final mass of 0.05–0.14 $\rm M_\oplus$.

As there are no major changes to the dynamical processes in the system after the LHB, we assume that the dynamical losses affecting the rest of the particles (for which we use the term primordial scattered disc) remain the same and so the total mass will continue to decline. Therefore, we can extrapolate the mass evolution to the present day and into the future (Fig. 2). From ∼950 Myr onwards, the total mass (in Earth masses) as a function of time (in Myr) can be fitted by the equation

$$M_{\rm tot} = \frac{3.6}{[1 + (t - 995)/280]^2} + M_{\rm CKB}, \quad (1)$$

which puts the current total mass at 0.03 $\rm M_\oplus$ and the mass in the primordial scattered disc at 0.02 $\rm M_\oplus$, which agrees well with the observations that set the current mass of the scattered disc to between 0.01 and 0.1 $\rm M_\oplus$ (Gomes et al. 2008, and references therein). The evolution of the total mass of KBOs in the system is shown in Fig. 2, which also shows the constant component of the CKB and the depleting component of the primordial scattered disc, which combine to make up the total extrapolated mass.

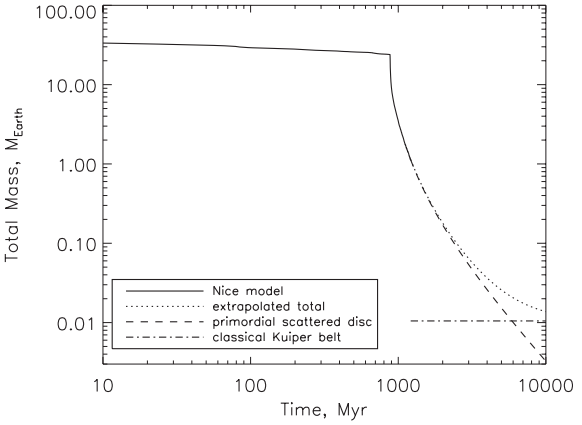

Figure 2. Total mass of KBOs in the Nice model and extrapolated mass beyond the Nice model using equation (1). The scattered disc (dashed line) and classical belt (dot–dashed line) contributions to the total extrapolated mass are also shown.

2.3 Converting mass to dust emission

Each particle in the simulation represents a collection of KBOs of many different sizes, which are assumed to be affected by dynamical perturbations in the same way. By making some assumptions about the size distribution of the objects (which will be considered in more detail in Section 3.1), we can work out the cross-sectional area of dust corresponding to the mass in each radius bin and thus, the flux emitted from these particles.

First, we assume that a collisional cascade is set up quickly (from $t = 0$) and so the planetesimals are in collisional equilibrium with a differential size distribution of the form $n(D) \propto D^{2-3q_{\rm d}}$ where D is the diameter of the particles (in km) and $q_{\rm d} = 11/6$ for an infinite collisional cascade (Dohnanyi 1968). This size distribution is assumed to apply from the largest objects of size $D_{\rm c}$ down to the smallest particles of size $D_{\rm bl}$. Particles smaller than this are created in collisions between larger objects but are blown out of the system by radiation pressure on dynamical time-scales and so contribute little to the size distribution.

Taking $q_{\rm d} = 11/6$, $D_{\rm c} = 2000$ km, $D_{\rm bl} = 2.2\ \mu$m and the particle density, $\rho = 1000\ {\rm kg\ m^{-3}}$, we find that the total cross-sectional area in each radius bin [$\sigma(R)$ in au^2] is related to the total mass in each radius bin [$M(R)$ in $\rm M_\oplus$] by

$$\frac{\sigma(R)}{M(R)} = 0.19\ {\rm au^2 M_\oplus^{-1}}. \quad (2)$$

As a first approximation, we assume that the particles act like perfect blackbodies, except at submillimetre wavelengths where an additional modification is applied. This is fine for large grains but does not work for small grains. Improvements to this assumption will be considered in Section 3. Using the blackbody emission from the particles and the cross-sectional area worked out in equation (2) we can find the flux density (in Jy) measured by a distant observer:

$$F_\nu = \sum_R 2.35 \times 10^{-11} \sigma(R) B_\nu(\lambda, T_{\rm bb}(R)) d^{-2} X_\lambda^{-1} \quad (3)$$

$$T_{\rm bb}(R) = 278.3 L_\star^{1/4} R^{-1/2}, \quad (4)$$

where B_ν is the Planck function (in units of Jy sr^{-1}), which is dependent on the wavelength and temperature, d is the distance to the observer (in pc), $L_\star$ is the luminosity of the star (in units of $\rm L_\odot$), R is the distance between the particle and the star (in au) and X_λ

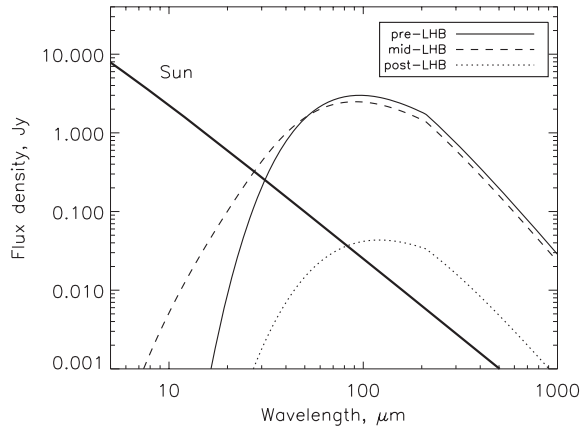

Figure 3. SED before, during and after the LHB, as it would appear from 10 pc away. The thick line shows the solar photosphere. The thin lines show the excess emission at 873, 881 and 1212 Myr. The total emission spectrum observed would be the sum of the photosphere and excess.

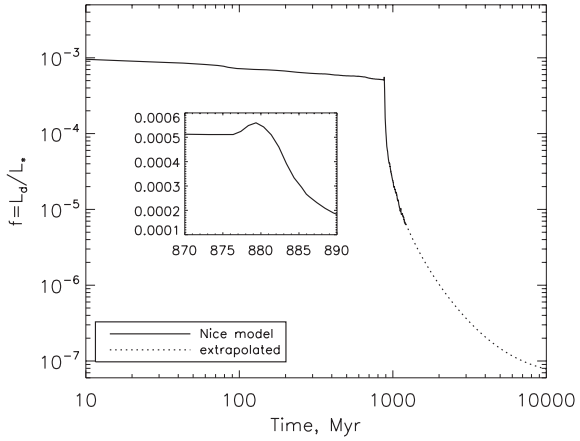

Figure 4. Fractional luminosity as a function of time. Inset shows small increase in fractional luminosity during the LHB. However, it should be noted that the peak is diminished due to the fact that we have averaged over 5 Myr (see Section 2.2). The fractional luminosity at late times is an overestimate since we have ignored PR drag and SW drag effects (see Section 2.5.2).

is a factor that accounts for the drop off in the emission spectrum beyond ∼200 μm. Here, we take $X_\lambda = 1$ for $\lambda < 210\,\mu$m and $X_\lambda = \lambda/210$ for $\lambda \geq 210\,\mu$m to be consistent with submillimetre observations of extrasolar debris discs (see Wyatt et al. 2007b). The numerical coefficient in equation (3) arises because different units are used for different parameters, an approach employed throughout the paper.

By plotting the flux density against wavelength for the dust emission (see Fig. 3), we can see how the LHB causes the emission spectrum to change. Before the LHB, the emission resembles a single temperature spectrum appropriate to the radius of the belt (i.e. 55 K at 26 au). During the LHB, the spreading of mass from the belt (see Fig. 1) means that the dust is emitting from a much broader range of temperatures and so the spectrum covers a broader range of wavelengths. Wavelengths as low as 7 μm now have a flux density $>10^{-3}$ Jy as opposed to just wavelengths 16 μm and longer in the pre-LHB phase. In particular, we see that the mid-infrared (IR) flux is enhanced. After the LHB has occurred, the flux at all wavelengths rapidly decreases and the spectrum begins to resemble a single temperature blackbody once again but at a longer peak wavelength due to the increase in mean radius of the belt.

The increase in mid-IR flux seen here during the LHB is only a lower limit, since objects with perihelion less than 1 au are removed from the simulation, which removes a lot of planetesimals that are scattered on to cometary orbits (as discussed in Section 2.2). These would otherwise contribute to the emission via dust production and sublimation. We also note that the true mid-IR emission may be higher at all times as we have only considered the contribution of the Kuiper belt and have not included the asteroid belt. These effects will be investigated in more detail in future work.

Flux density is dependent on distance from the observer to the star. To be able to compare different debris discs, it is necessary to use a variable independent of distance. As stellar flux density (in Jy) is also $\propto d^{-2}$:

$$F_{\nu\star} = 1.77 B_\nu(\lambda, T_\star) L_\star T_\star^{-4} d^{-2}, \tag{5}$$

the excess ratio ($F_\nu/F_{\nu\star}$, also called the fractional excess) is one distance independent measure, but is dependent on wavelength. A variable independent of both distance and wavelength is the fractional luminosity, f, which measures the ratio of the excess luminosity (due to the dust) to the luminosity of the star:

$$f = \frac{L_\mathrm{d}}{L_\star} = \frac{\int F_\nu \mathrm{d}\nu}{\int F_{\nu\star} \mathrm{d}\nu}, \tag{6}$$

where L_d is the luminosity of the dust and $L_\star$ is the luminosity of the star.

Fig. 4 shows how fractional luminosity varies with time for our model. Before the LHB event, the fractional luminosity shows that the planetesimal disc is in a quasi-steady state in that dynamical losses of KBOs are a relatively small fraction of the total mass. At the time of the LHB, there is a slight but minimal increase in f due to the influx of comets. After the LHB, f rapidly decreases in a similar manner to M_tot (see Fig. 2). Here we assume that the radial distribution of the mass remains the same from the end of the Nice model. In reality, since the mass of the CKBOs remains constant and it is only the SDOs that are being lost through dynamical processes (see Section 2.2), the distribution of mass will again resemble a narrow belt similar to that present before the LHB but at a larger radius. As such this assumption probably overestimates the mid-IR flux at late times because there would not be as much mass spread inwards as we are assuming.

By extrapolating the fractional luminosity, we find that this model gives the current value to be $f = 2 \times 10^{-7}$ which is within the range 10^{-7}–10^{-6} suggested by the size distribution of KBOs (Backman, Dasgupta & Stencel 1995; Stern 1996b).

2.4 Comparison with extrasolar debris discs

Dust in debris discs emits most strongly in the IR, as can be seen in Fig. 3. Since its launch in 2003, the *Spitzer Space Telescope* has been used to survey stars for IR excesses. The Multiband Imaging Photometer for *Spitzer* (MIPS) makes observations of the stars at 24 and 70 μm which can then be compared to photospheric models to calculate if there is evidence for any excess emission which may be due to dust present in the system. Surveys using *Spitzer* are generally calibration limited, which means that they can detect stars with a fractional excess (the ratio of flux from the dust to flux from the star at a given wavelength) above a given limit. At 24 μm, the Formation and Evolution of Planetary Systems (FEPS) survey can make 3σ detections of excess down to a limit of $F_{24}/F_{24\star} = 0.054$

for the brightest stars (Carpenter et al. 2009). At 70 μm, the limit is approximately $F_{70}/F_{70\star} \approx 0.55$, although observations of the more distant stars are sensitivity limited and so have not been observed down to this limit (Wyatt 2008).

Carpenter et al. (2009) surveyed 314 stars and found that there is a decrease in 24 μm excess with age. They show that 15 per cent of stars younger than 300 Myr have a 24 μm excess greater than 10.2 per cent above the photosphere but this fraction goes down to 2.7 per cent for older stars. By combining observations of both field stars and stars in open clusters and associations from the literature, Gáspár et al. (2009) also find that there is a decrease in the fraction of stars with 24 μm excess with age, levelling off at a few per cent for stars older than 1 Gyr. Trilling et al. (2008) found that 16 per cent of F- and G-type stars have detectable debris discs at 70 μm from a sample of 225 stars. Although they show that the data could indicate a decrease in the fraction of stars with detectable excess with age, a constant excess fraction also adequately fits the data and there are currently too few observations to distinguish between the two. Hillenbrand et al. (2008) similarly find no apparent trend in the 70 μm excess fraction with age; however they do note that the maximum excess ratio at 70 μm does appear to decrease with age, which can be seen in Fig. 5 (bottom).

The evolution of the fractional excesses at 24 and 70 μm for our model are shown in Fig. 5. For comparison, these plots also show 106 Sun-like stars (represented by asterisks) for which excesses have been detected (Habing et al. 2001; Beichman et al. 2006; Moór et al. 2006; Trilling et al. 2007; Hillenbrand et al. 2008; Trilling et al. 2008; Carpenter et al. 2009). 77 of these stars have observed excesses at 70 μm and 53 of them have observed excesses at 24 μm. The dashed lines show the approximate limits of detectability.

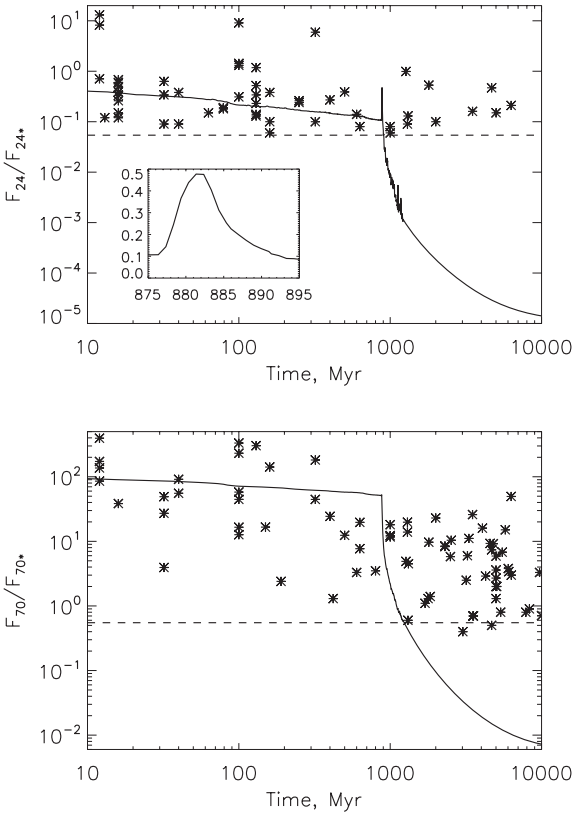

Figure 5. Excess ratio versus time for 24 (top) and 70 μm (bottom). The solid line represents the emission from our model, assuming a single-slope size distribution with $q_{\rm d} = 11/6$ and blackbody grains (cf. Fig. 12). The asterisks are observed discs and the dashed line shows the approximate observational limit. The excess ratio at late times is an overestimate since we have ignored PR drag effects (see Section 2.5.2).

From the 24 μm excess, we can see that the hot emission from the model starts at $F_{24}/F_{24\star} = 0.5$, which is high enough to make the Kuiper belt detectable at early times. This hot emission gradually decreases during the pre-LHB phase and then briefly rises again during the LHB back to its initial value (see inset of Fig. 5, top) due to an increase in the mass closer to the Sun (see Fig. 1). The Kuiper belt is also detectable at 70 μm at early times. The 70 μm excess remains in a quasi-steady state until the LHB at which point it drops off sharply, but still remains detectable up to 360 Myr after the LHB.

It is possible that some of the observed systems may be going through a similar process and that some systems may be observed whilst in the middle of an LHB-like epoch, especially those systems described in Wyatt et al. (2007a) as having a mid-IR excess (from dust at a few au) higher than expected for their age. However, it is unlikely to explain systems like HD 69830 which have been detected at 24 μm but not at 70 μm since our results imply that, although the 70 μm excess of a system does decrease from the time of the LHB onwards, the system should still be detectable at 70 μm for a few hundred million years after the LHB. In other words, a system must have a significant cold disc at the same time as the hot disc to provide material for the hot disc.

Fig. 5 (bottom) shows that there are a large number of observed discs at late times, which clearly have not gone through an LHB. The fact that the Trilling et al. (2008) results are consistent with the fraction of Sun-like stars with a detectable 70 μm excess remaining approximately constant with age at $16.4^{+2.8}_{-2.9}$ per cent shows that extrasolar LHB events must be rare. Although, the number of systems surveyed is still fairly low, we can still place an upper limit on the fraction of systems that may undergo an LHB event. To get this limit, we start by assuming that if a star is born with a planetesimal belt that is detectable at 70 μm then it remains detectable unless a major planetesimal-clearing event, like an LHB, takes place. For the fraction of stars born with a detectable planetesimal belt, we assume that the value of $16.4^{+2.8}_{-2.9}$ per cent from Trilling et al. (2008) also applies at the youngest ages (<100 Myr). Although the Trilling sample is not focused on young stars, not including any systems younger than 100 Myr, the results of Carpenter et al. (2009) are consistent with the distribution of fractional excesses remaining constant for all ages.[1] Thus, the lack of decline tells us that the fraction of stars starting with a 70 μm excess that go through a planetesimal-clearing event is 0 per cent with a 3σ upper limit of $3\sqrt{2(2.9/16.4)^2} = 75$ per cent. This gives a maximum of 12 per cent of all Sun-like stars experiencing an LHB event.

Since we might expect an LHB event to require the presence of giant planets, it is encouraging to find that this fraction is not greater than the fraction of Sun-like stars inferred to have gas giants (planets with masses equal to or greater than Saturn) within 20 au which Marcy et al. (2005) estimate as 12 per cent. If LHBs were common for stars with giant planets, then the presence of debris would be expected to be anti-correlated with the presence of giant planets for old stars. Since this is not observed to be the case (Greaves et al.

[1] Note that a direct comparison of the fraction of stars detected in each of these surveys is not possible since stars in the different surveys were observed down to different levels of fractional excess, notably with higher detection thresholds for the young stars in the Carpenter survey which are typically at greater distance.

2004a) and several old stars are now known with both giant planets and debris (see table 1 in Moro-Martín et al. 2007, where all the stars are at least 500 Myr), this is further evidence that the fraction of stars that undergo LHBs is <12 per cent (assuming that Saturn mass planets within 20 au are required for an LHB).

Gáspár et al. (2009) also estimate the fraction of Sun-like stars that go through an LHB event. They find a maximum limit of 15–30 per cent based on observations of 24 μm excess. This is much higher than our own limit as they have been less restrictive with their definition of an LHB event. They assume that any star that is observed to have a 24 μm excess must be going through an LHB, however we have shown that debris discs can be detectable at 24 μm in the pre-LHB phase (see Fig. 5, top). Furthermore, only a small number of systems have a 24 μm excess that is too high to be explained by collisional processing (Wyatt et al. 2007a).

Observations in the submillimetre part of the spectrum offer a useful method for estimating the dust mass of debris discs and so are often used as another method of comparing debris discs. The dust mass, $M_{\rm dust}$ in $M_\oplus$, can be calculated using (e.g. Zuckerman 2001)

$$M_{\rm dust} = 4.26 \times 10^{10} F_\nu d^2 \kappa_\nu^{-1} B_\nu^{-1}, \quad (7)$$

where κ_ν is the mass absorption coefficient (in au^2 $M_\oplus^{-1}$). By combining this with equation (3), we find that

$$M_{\rm dust} = \sum_R \sigma(R) \kappa_\nu^{-1} X_\lambda^{-1}. \quad (8)$$

There is a lot of uncertainty in the value of κ_ν since it is dependant on the properties of the particles in the system. Here we adopt the value $\kappa_{850\mu{\rm m}} = 45$ au^2 $M_\oplus^{-1}$ to ease comparison with values reported elsewhere (Najita & Williams 2005). Fig. 6 shows the submillimetre dust mass predicted by our model. The asterisks represent dust masses for Sun-like stars that have been observed to have an excess at 850 μm. Data for these 13 stars are taken from the literature (Wyatt, Dent & Greaves 2003; Greaves et al. 2004b, 2005; Sheret, Dent & Wyatt 2004; Najita & Williams 2005; Wyatt et al. 2005; Williams & Andrews 2006; Greaves, Wyatt & Bryden 2009).

Greaves et al. (2004b) use *COBE*/FIRAS (Far-Infrared Absolute Spectrometer) observations at 800 μm to provide an upper limit to the dust mass of the Kuiper belt, which they find to be $\sim 2 \times 10^{-5}$ $M_\oplus$. Our model implies that the current dust mass is $\sim 3.1 \times 10^{-5}$ $M_\oplus$. The discrepancy between our result and the observations may be due to Poynting–Robertson (PR) drag being neglected in our model, which can have the effect of reducing the amount of small dust in a debris disc as described in Section 2.5.2.

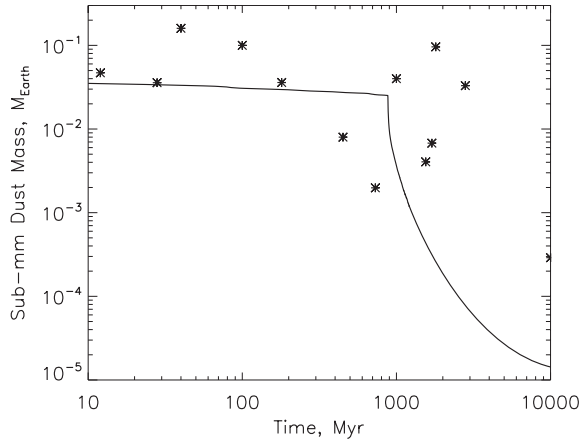

Figure 6. Sub-mm dust mass as a function of time. The solid line represents the emission from our model and the asterisks are observed discs around F, G and K stars. The dust mass at late times is an overestimate since we have ignored PR drag effects (see Section 2.5.2).

2.5 Collisional lifetime

Mass loss in the Nice model is entirely due to the dynamical evolution of the particles. For computational reasons, it was assumed that the particles only interacted with the planets and not with each other. In reality, collisional processes are likely to have had some effect on mass loss in the system. In this section, we investigate the effect of collisions and PR drag on our simple model.

In Section 2.3, we assumed that the particles are in a collisional cascade. In a collisional cascade, objects of size D to $D + dD$ are destroyed by collisions only to be replaced by fragments created by collisions of larger objects. From the equations of Wyatt et al. (1999, 2007a), it can be shown that the time between catastrophic collisions (known as the collision time-scale) for particles of size D in a belt at a mean distance $R_{\rm m}$ (in au) from the star and with a width dr (in au) is given by

$$t_{\rm c}(D) = \left(\frac{R_{\rm m}^{2.5} dr}{M_\star^{0.5} \sigma_{\rm tot}} \right) \left\{ \frac{2[1 + 1.25(e/I)^2]^{-0.5}}{f_{\rm cc}(D)} \right\}, \quad (9)$$

$$\sigma_{\rm tot} = \frac{\sigma(R)}{M(R)} M_{\rm tot}, \quad (10)$$

where $t_{\rm c}$ is in years, $M_\star$ is the mass of the star in solar masses, $\sigma_{\rm tot}$ is the total surface area and e and I are the mean of the eccentricities and mean of the inclinations (in radians), respectively. $f_{\rm cc}(D)$ is a factor determined by the fraction of the total cross-sectional area which is seen by a particle of size D as potentially causing a catastrophic collision and is given by

$$f_{\rm cc}(D) = \int_{D_{\rm cc}(D)}^{D_{\rm c}} (1 + D/D')^2 \bar{\sigma}(D') {\rm d}D', \quad (11)$$

where $D_{\rm cc}(D)$ is the smallest particle that can catastrophically destroy a particle of size D and $\bar{\sigma}$ is the normalized cross-sectional area distribution in each diameter bin. Since we are assuming a single power law with $q_{\rm d} > 5/3$, this can be written as

$$f_{\rm cc}(D) = \frac{3q_{\rm d} - 5}{D_{\rm bl}^{5-3q_{\rm d}}} \left\{ \frac{D_{\rm cc}(D)^{5-3q_{\rm d}} - D_{\rm c}^{5-3q_{\rm d}}}{3q_{\rm d} - 5} + \frac{2D \left[D_{\rm cc}(D)^{4-3q_{\rm d}} - D_{\rm c}^{4-3q_{\rm d}} \right]}{3q_{\rm d} - 4} + \frac{D^2 \left[D_{\rm cc}(D)^{3-3q_{\rm d}} - D_{\rm c}^{3-3q_{\rm d}} \right]}{3q_{\rm d} - 3} \right\}, \quad (12)$$

$D_{\rm cc}(D) = X_{\rm c} D$ for $X_{\rm c} D > D_{\rm bl}$ and $D_{\rm cc}(D) = D_{\rm bl}$ otherwise. The factor $X_{\rm c}$ can be calculated using the equation

$$X_{\rm c} = 1.3 \times 10^{-3} \left[Q_{\rm D}^\star R_{\rm m} M_\star^{-1} f(e, I)^{-2} \right]^{1/3}, \quad (13)$$

where $Q_{\rm D}^\star$ is the dispersal threshold and $f(e, I)$ is the ratio of relative velocity to Keplerian velocity. This is given by

$$f(e, I) = \sqrt{1.25e^2 + I^2}. \quad (14)$$

Here, we use the value $Q_{\rm D}^\star = 200$ J kg^{-1} since this value provides a good fit to the statistics of debris discs around A stars (Wyatt et al. 2007b). This is an effective planetesimal strength that describes the dust mass-loss rate from the planetesimal belt, which is linked to medium-sized planetesimals (e.g. $D_{\rm c} = 160$ km in Wyatt et al. 2007b). In reality, $Q_{\rm D}^\star$ varies with size. Thus, we expect to derive a collisional lifetime that is reasonably accurate with regards the

evolution of the IR emission and of the planetesimal belt mass, but note that the collisional lifetime of objects of a specific size will not be quantitatively correct. In Section 3.1, we investigate the effects of including a more realistic dispersal threshold that is dependent on size.

Although the planetesimals in our model are not confined to a uniform ring for the entirety of the Nice model, we can still use this model to estimate the collisional lifetime by making the assumption that $R_{\rm m}$ is the radius containing half of the mass of the disc, dr is the annuli containing 98 per cent of the mass and using the mean eccentricities and mean inclinations from the Nice model data.

The mean radius of the belt is approximately constant at 26 au during the pre-LHB phase and then rises during the LHB due to the planetesimals being scattered and reaches 79 au. Similarly, the width of the belt is approximately 17 au during the pre-LHB phase and rises to a maximum of 640 au after the LHB. The radius and width of the belt at the end of the simulation are clearly much larger than the present day classical Kuiper belt. This is because most of the objects left at the end of the simulation are SDOs with a range of (typically high) eccentricities. Thus, our assumption that the planetesimals are confined to a uniform ring clearly does not hold after the LHB, and moreover a range of collisional lifetimes would be expected depending on the objects' orbits. Nevertheless, we note that the collision time-scale derived above is within 25 per cent of that expected for an eccentric ring of planetesimals all with semimajor axes at 102 au and eccentricities of 0.56, which are the mean values from the simulation at the end of the post-LHB phase (Wyatt et al. 2009). Thus, we expect the post-LHB collisional lifetimes presented here to be representative of an average member of the scattered disc in this phase, but use this simply to note that the collisional lifetime rapidly becomes larger than the age of the Solar system so that there is no further collisional mass loss (in agreement with Levison et al. 2008b). A consideration of collision rates in populations with a range of eccentricities and semimajor axes (see Wyatt et al. 2009) would be required for a more detailed understanding of collision lifetimes in the post-LHB population.

The mean eccentricities and inclinations give a mean relative velocity of around 360 m s^{-1} for the time before the LHB. At the time of the LHB, the large number of planetesimals being scattered leads to a rapid increase in the mean relative velocity, which rises to a maximum of 2700 m s^{-1} at 900 Myr. After this time, the mean relative velocity gradually decreases to a value of 2500 m s^{-1} at the end of the simulation as the highly eccentric and inclined particles are more likely to be scattered out of the system.

2.5.1 *Collisional lifetime of the largest objects*

As discussed above, $Q_{\rm D}^\star$ should be much greater than 200 J kg^{-1} (e.g. Benz & Asphaug 1999) for the largest objects (of size 2000 km); however, we can still use this model to estimate qualitatively the evolution of mass due to collisions. Fig. 7 shows how the collision time-scale of the largest objects changes as the system evolves. The time-scale has been extrapolated assuming that the total mass is the only parameter in equation (9) that changes with time after the end of the Nice model simulation as described in Section 2.2. During the pre-LHB period, we find that the collision time-scale varies between 100 and 300 Myr. This implies that catastrophic collisions might have played a significant role in mass loss before the LHB. Since we need to end up with 24 $M_\oplus$ of KBOs at the beginning of the LHB (see Section 2.1), we can approximate how massive the initial disc must have been to account for collisional mass loss. If we assume that before the LHB all the mass was lost

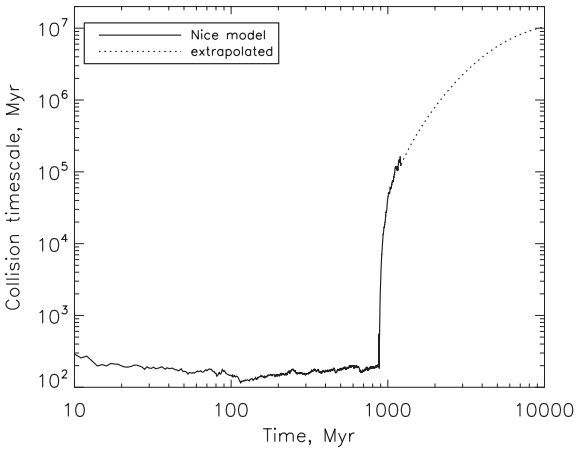

Figure 7. Collision time-scale of the largest (Pluto-sized) objects as a function of time. Catastrophic collisions are only important before and during the LHB. The actual time-scales shown here are unrealistically small due to the assumption of a size-independent dispersal threshold.

through collisions then the total mass evolves as (e.g. Wyatt et al. 2007a)

$$M_{\rm tot} = M_{\rm init}/[1 + t/t_c(D_{\rm c})]. \quad (15)$$

This means that we require an initial mass of $\sim$150 $M_\oplus$ to account for the mass lost due to collisions. By taking into account the mass lost through dynamical processes ($\sim$10 $M_\oplus$), this gives us a rough estimate of 160 $M_\oplus$ as the initial mass of the Kuiper belt, much greater than the 35 $M_\oplus$ used in Gomes et al. (2005). Although this is a very rough approximation of the collisional evolution and these results are not quantitatively correct due to the assumption of a size-independent dispersal threshold (which will be considered in more detail in Section 3), it does show us that collisions were important before the LHB and so would have affected the evolution of mass in the system.

After the instability, the collision lifetime increases to beyond the lifetime of the Solar system, with a collision lifetime of 130 Gyr by the end of the simulation and 5000 Gyr by the present day. This shows that collisions of the largest bodies become so infrequent that they can be neglected.

2.5.2 *Lifetimes of the smallest particles*

In Section 2.3, we assumed that the cut-off at the small end of the size distribution was defined by radiation pressure – particles smaller than $D_{\rm bl}$ will be blown out of the system by radiation pressure. However, particles larger than this may be affected by PR drag or solar wind (SW) drag on shorter time-scales than those for removal by collisions. To assess this, we first calculate the collision time-scales using equation (9) for particles of size $D_{\rm bl}$. This gives a time-scale that evolves similar to the time-scale for the largest objects but up to 5 orders of magnitude shorter (Fig. 8).

PR drag is the tangential component of the radiation force, which causes a decrease in both the semimajor axis and the eccentricity of a particle. The time-scale for a particle of size $D_{\rm bl}$ to spiral into the Sun from a distance $R_{\rm m}$ under the influence of PR drag is given by (Wyatt et al. 1999)

$$t_{\rm PR} = 400 \frac{{\rm M}_\odot}{M_\star} \frac{R_{\rm m}^2}{\beta}, \quad (16)$$

where $\beta = 0.5$ for the smallest grains.

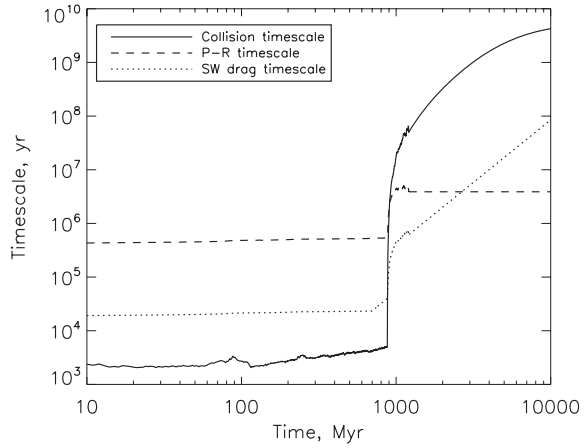

Figure 8. Collision, PR drag and SW drag time-scales of the smallest particles (2.2 μm) as a function of time. These time-scales assume that the particles are confined to a belt with a mean radius that increases due to the scattering caused by the LHB as described in the text. The PR drag and SW drag time-scales become important after the LHB.

A similar effect is caused by the tangential component of the SW known as the corpuscular stellar wind drag (hereafter SW drag). At the present time, the SW drag force is equivalent to only 20–43 per cent of the PR drag force (Gustafson 1994); however, the higher mass-loss rate of the young Sun means that SW drag would have been more effective at removing dust than PR drag at early times (Minato et al. 2006). The ratio of the SW drag time-scale to the PR drag time-scale is given by (Plavchan, Jura & Lipscy 2005)

$$\frac{t_{\rm SW}}{t_{\rm PR}} = 3.4 \frac{Q_{\rm PR}}{Q_{\rm SW}} \frac{\dot{M}_\odot}{\dot{M}_\star} \frac{L_\star}{\rm L_\odot}, \tag{17}$$

where $Q_{\rm PR}/Q_{\rm SW}$ is the ratio of the coupling coefficients, $\dot{M}_\odot$ is the present day mass loss of the Sun and $\dot{M}_\star$ is the mass loss of the Sun at different epochs.

For this paper, we have assumed that $Q_{\rm PR}/Q_{\rm SW} = 1$, $\dot{M}_\odot = 2\times10^{-14}\,{\rm M_\odot\,yr^{-1}}$ and the luminosity remains constant at $1\,{\rm L_\odot}$. Although the luminosity of the Sun has changed with time and is likely to have been only $0.7\,{\rm L_\odot}$ when it first became a main-sequence star (e.g. Jorgensen 1991, and references therein), the uncertainties in the other factors in this equation are much greater than those due to this change in luminosity. For the change in stellar mass-loss rate with time, we have taken $\dot{M}_\star(t) = \dot{M}_\odot(t/4.5\,{\rm Gyr})^{-2.33}$ for $t >$ 700 Myr from the analysis of stellar mass-loss rates in Wood et al. (2005) and $\dot{M}_\star(t) = 80\,\dot{M}_\odot$ for earlier times.

Fig. 8 compares the collision time-scale with the PR drag time-scale and the SW drag time-scale for particles of size $D_{\rm bl}$. Collisional processes would have dominated the removal of dust before the LHB due to the high dust mass present and the compactness of the belt. Drag forces would have been insignificant as they are in all other observed debris discs (Wyatt 2005). However, as the distribution of mass becomes increasingly spread out during and after the LHB, the collision time-scales of the particles rapidly increase such that they become more susceptible to drag forces. Due to the high mass-loss rate of the early Sun, SW drag is more effective at removing dust than PR drag until ∼2.7 Gyr. The increased rate of dust removal due to drag forces throughout the post-LHB phase reduces the amount of small dust below that expected in the collisional cascade equation (10). This means that the collisional lifetime of the smallest particles is in fact underestimated in Fig. 8 (which assumes the collisional cascade size distribution extends down to the blow-out limit). Since it is the smallest dust that contributes most to the emission, this increased rate of dust removal also reduces the emission and means that we have overestimated the fractional luminosity (shown in Fig. 4) and the observable properties dependent on this (Figs 5 and 6) at late times. However, since it is predicted that the Kuiper belt would not be observable at this time (Figs 5 and 6), this does not affect the comparison with observed debris discs.

We note that the time-scales used here are all for the average particles in the model. In the pre-LHB phase, some particles are occasionally scattered in from the narrow belt making them more susceptible to drag forces. During and after the LHB, the range of orbital elements of the particles is greatly increased. Since both of the drag forces are proportional to $R_{\rm m}^2$, the position of a particle will greatly affect whether it is destroyed through collisions or spirals into the Sun due to drag forces.

We also note that the mass-loss rate of the Sun at early times is not very well constrained. Some authors (e.g. Sackmann & Boothroyd 2003) have suggested that the mass-loss rate of the Sun in the early Solar system may have been as much as 1000 times greater than the current value. If the mass-loss rate was this high then the SW drag time-scale would have been shorter than the collisional time-scale for the smallest particles reducing the small size end of the size distribution, thus reducing the luminosity of the disc in the pre-LHB phase below that presented here.

3 REALISTIC SIZE DISTRIBUTION AND GRAIN PROPERTIES

In Section 2, we described a basic method for investigating the history of the Solar system's debris disc. That modelling method can readily be applied to the outcome of any numerical simulation to consider its observable properties. In this section, we will confront two of the main assumptions of the model. So far, we have been assuming that the planetesimals and dust are governed by a single-phase size distribution and that they are blackbodies (with a slight correction at sub-mm wavelengths).

3.1 Three-phase size distribution

In Section 2.3, we assumed that the particles are in a collisional equilibrium from the smallest to the largest particle. Using their collisional evolution code, Löhne et al. (2008) show that a disc that starts with a single power-law size distribution will quickly develop into a system with a three-phase power law due to differences in the collisional time-scales of different sized particles. As the system evolves (Fig. 9), the particles begin to reach collisional equilibrium starting with the smallest particles due to their shorter collisional lifetime (see Section 2.5). The transition diameter, $D_{\rm t}$, defines the diameter at which the collisional lifetime of the particles is equal to the age of the system. Particles below this size will reach collisional equilibrium. The slope of the power law for particles smaller than $D_{\rm t}$ will then depend on whether the particles are in the strength or gravity regimes. The slope of the power law for particles larger than $D_{\rm t}$ is given by the primordial slope, $q_{\rm p}$.

In Section 2.5, we assumed that the dispersal threshold of a particle is independent of its size. This dispersal threshold defines the minimum energy required to catastrophically destroy a planetesimal and disperse the fragments such that they do not recombine under their own gravity and is, in fact, dependent on the size of the particle. The dispersal threshold decreases with size for the smallest size particles for which little energy is required to disperse the fragments after the collision (the strength regime, see e.g. Farinella,

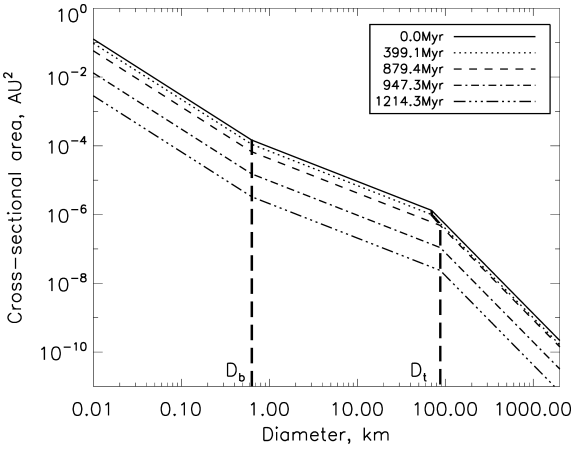

Figure 9. Evolution of the size distribution for an initial transition diameter of 70 km and initial mass of 40 $M_\oplus$. The size distribution continues down to $D_{\rm bl}$ but this has not been shown for clarity. The thick dashed lines represent the break diameter and the transition diameter. There is some increase in $D_{\rm t}$ pre-LHB when mass is being lost through collisions but the size distribution then remains fixed from the onset of the LHB and all the mass lost after this time is due to dynamics.

Paolicchi & Zappala 1982; Housen & Holsapple 1990; Benz & Asphaug 1999). As object size increases so does the gravitational strength (assuming constant density) to the extent where the energy required to disperse the fragments of a collision is greater than the energy required to catastrophically destroy the planetesimal. For these objects, the dispersal threshold increases as size increases (the gravity regime, see e.g. Petit & Farinella 1993; Campo Bagatin, Farinella & Petit 1994; Benz & Asphaug 1999). These two regimes can be described by the sum of two power laws (e.g. Krivov, Sremčević & Spahn 2005):

$$Q^\star_{\rm D}(D) = A_{\rm s}\left(\frac{D}{2\,{\rm m}}\right)^{3b_{\rm s}} + A_{\rm g}\left(\frac{D}{2\,{\rm km}}\right)^{3b_{\rm g}}, \tag{18}$$

where $A_{\rm s}$, $A_{\rm g}$, $b_{\rm s}$ and $b_{\rm g}$ are free parameters. This equation can then be used to find the transition between the strength and gravity regimes (the diameter at which the two power-law components contribute equally), which occurs at the breaking diameter, $D_{\rm b}$ (in km):

$$D_{\rm b} = \left[\frac{A_{\rm s}}{A_{\rm g}}\frac{2^{3b_{\rm g}}}{(2\times10^{-3})^{3b_{\rm s}}}\right]^{1/(3b_{\rm g}-3b_{\rm s})}. \tag{19}$$

To find $D_{\rm t}$ we assume that the disc starts as a single power law with a primordial distribution given by $q_{\rm p}$. Using equation (9) (and adjusting $\sigma_{\rm tot}$ and $f_{\rm cc}$ for a three-phase distribution), we can find the diameter for which an object's collisional time-scale is the same as the age of the system, $t_{\rm c}(D_{\rm t}) = t$. Objects smaller than $D_{\rm t}$ will be governed by either the strength regime (if their size is also below $D_{\rm b}$) with a slope of $q_{\rm s}$ or the gravity regime with a slope of $q_{\rm g}$.

If we know the transition diameter at a particular time, then we can work out the total mass of the disc at that time:

$$M_{\rm totl}(t) = 8.7\times10^{-17} n_{\rm max}(t)\rho B(t), \tag{20}$$

$$n_{\rm max}(t) = \frac{n_{\rm max}(0)}{1 + t/t_{\rm c}(D_{\rm c})}, \tag{21}$$

$$B(t) = \left\{\frac{D_{\rm t}(t)^{3q_{\rm g}-3q_{\rm p}} D_{\rm b}^{3q_{\rm s}-3q_{\rm g}}}{6-3q_{\rm s}}\left(D_{\rm b}^{6-3q_{\rm s}} - D_{\rm bl}^{6-3q_{\rm s}}\right) + \frac{D_{\rm t}(t)^{3q_{\rm g}-3q_{\rm p}}}{6-3q_{\rm g}}\left[D_{\rm t}(t)^{6-3q_{\rm g}} - D_{\rm b}^{6-3q_{\rm g}}\right] + \frac{D_{\rm c}^{6-3q_{\rm p}} - D_{\rm t}(t)^{6-3q_{\rm p}}}{6-3q_{\rm p}}\right\}, \tag{22}$$

where $n_{\rm max}$ is the number of objects of size $D_{\rm c}$ and assuming that none of $q_{\rm s}$, $q_{\rm g}$ and $q_{\rm p}$ are equal to 2. Given the parameters of our model, we find that the largest objects can only be destroyed by objects much larger than themselves and so cannot be collisionally destroyed in any of our simulations (see Section 3.1.2) allowing us to ignore the $t/t_{\rm c}(D_{\rm c})$ term.

However, since $D_{\rm t}(t)$ is dependent on $M_{\rm totl}(t)$ (through equations 9 and 10), $D_{\rm t}$ is calculated at each time-step based on the total mass of the previous time-step. If we ignore the dynamical mass loss from the system, then the total mass at each time-step is given by

$$M_{\rm totl}(t_n) = M_{\rm totl}(t_{n-1})\frac{B(t_n)}{B(t_{n-1})}. \tag{23}$$

If we assume that the collisional evolution does not affect the rate of mass lost from dynamical evolution, then the dynamical evolution of the Nice model (as described in Section 2.2) can be combined with this equation to give us a total mass, $M_{\rm totl}$, that evolves as

$$M_{\rm totl}(t_n) = M_{\rm totl}(t_{n-1})\left[\frac{B(t_n)}{B(t_{n-1})} - \frac{\Delta M_{\rm tot}(t_n)}{M_{\rm tot}(t_{n-1})}\right], \tag{24}$$

$$\Delta M_{\rm tot}(t_n) = M_{\rm tot}(t_n) - M_{\rm tot}(t_{n-1}). \tag{25}$$

By keeping our assumption that the cross-sectional area is proportional to the mass and that the proportionality constant is defined by the size distribution, the changing size distribution (Fig. 9) can then be used to find how the ratio of cross-sectional area to mass changes with time. This cross-sectional area can then be used to find the emitted flux as described for the basic model in Section 2.3.

3.1.1 Parameter choices

The free parameters in this model are $Q^\star_{\rm D}$, $q_{\rm p}$, $D_{\rm t}(0)$ and $M_{\rm totl}(0)$. Löhne et al. (2008) use a $Q^\star_{\rm D}$ similar to that of Benz & Asphaug (1999). For the coefficients they set $A_{\rm s} = A_{\rm g} = 500\,{\rm J\,kg^{-1}}$ and the exponents are $3b_{\rm s} = -0.3$ and $3b_{\rm g} = 1.5$. The transition between the strength and gravity regimes (the diameter at which the two power-law components contribute equally) occurs at the breaking diameter, $D_{\rm b} = 632$ m.

Leinhardt & Stewart (2009) show that, if comets have negligible strength, then their $Q^\star_{\rm D}$ function can be much lower than those of Löhne et al. (2008) and Benz & Asphaug (1999), with coefficients as low as $A_{\rm s} = 20\,{\rm J\,kg^{-1}}$ and $A_{\rm g} = 28\,{\rm J\,kg^{-1}}$ and exponents of $3b_{\rm s} = -0.4$ and $3b_{\rm g} = 1.3$, which gives a breaking diameter of $D_{\rm b} = 324$ m.

Stewart & Leinhardt (2009) go on to show that using $Q^\star_{\rm D}$ is only valid when the target object is much bigger than the object impacting it. When the impacting object is roughly half the size of the target object or larger (assuming impact and target have equal density), $Q^\star_{\rm D}$ is no longer valid as it only takes into account the size of the target object rather than the size of both objects. In our simulations, this means that objects of size $\gtrsim$130 km become harder to catastrophically destroy and objects $\gtrsim$440 km become impossible to destroy. However, as the objects most strongly affected by this

are bigger than the final transition diameter we are interested in, this does not make a significant difference to our work.

As the slope of the primordial distribution remains constant with time, this parameter can be found from present day observations. Recent surveys of the largest KBOs give a size distribution slope $q_p = 1.8 - 2.3$ (see Petit et al. 2008, and references therein). Although Bernstein et al. (2004) show that the classical belt and the excited belt have different size distributions, for this work we shall consider both populations to have the same size distribution. The most recent observations suggest a slope of $q_p \approx 2.2$ (Fraser & Kavelaars 2009; Fuentes, George & Holman 2009) and so we will use this value in the rest of this paper. q_s and q_g can be found from the formula (O'Brien & Greenberg 2003):

$$q = \frac{22/6 + b}{2 + b}, \tag{26}$$

which sets $q_s = 1.877$ and $q_g = 5/3$.

The initial conditions, $D_t(0)$ and $M_{totl}(0)$, are less well constrained. Löhne et al. (2008) start their model with a single size distribution and see how it evolves in to a three-phase size distribution. As the smallest particles have such a short collisional lifetime, the size distribution is likely to have already undergone some evolution before the time at which the Nice model begins and so $D_t(0) \gg D_{bl}$. Numerical simulations of the accretion of KBOs suggest that the initial transition diameter should be no less than 1 m and probably more than 100 m (Kenyon & Luu 1999). For the asteroid belt, it has been shown that the transition diameter is likely fixed during the accretion phase (Bottke et al. 2005). If the same is true of the Kuiper belt, then we would expect an initial transition diameter of ∼100 km. Models of formation of KBOs require that there must have been at least 10 $M_\oplus$ in the primordial Kuiper belt for the largest KBOs to have formed (e.g. Stern 1996a).

However, there are stronger constraints on the values of D_t and M_{totl} at the time of the LHB. The Nice model requires that there must be 24 $M_\oplus$ of planetesimals in the disc for the LHB to occur and that the size distribution becomes fixed at this time and so the transition diameter must be equal to the transition diameter in the current Kuiper belt. Observations constrain this diameter to between 50 and 200 km (Bernstein et al. 2004; Fraser & Kavelaars 2009; Fuentes et al. 2009). Taking these constraints into account, we can run the simulation with various initial conditions and find out which give the appropriate results.

The top plot of Fig. 10 shows simulation runs using the Löhne et al. (2008) $Q_D^\star$. The white region shows the runs which give a final transition diameter within the constraints of current observations and the 24 $M_\oplus$ line shows the runs which leave us with enough mass in the planetesimal belt for the LHB to occur. From this, we can see that if we start with a transition diameter $\gtrsim$100 km then there is no collisional mass loss since objects of this size have a collision time-scale longer than 879 Myr.

The bottom plot of Fig. 10 shows simulation runs using the Leinhardt & Stewart (2009) $Q_D^\star$. In these runs, the 24 $M_\oplus$ line does not overlap with the white area showing that we cannot satisfy both of our constraints with this $Q_D^\star$. This means that the Leinhardt & Stewart (2009) $Q_D^\star$ is inconsistent with the Nice model interpretation of the LHB as not enough mass remains in the Kuiper belt for the required length of time. This may be a result of our assumption that the dynamical evolution is not affected by the collisional evolution; it could mean that the objects are stronger than one would expect; or it might actually mean that the Nice model cannot be used to explain the LHB. To remain consistent with the Nice model interpretation of the LHB, we shall use the stronger $Q_D^\star$ throughout the rest of this paper. We will also set $q_p = 2.2$, $D_t(0) = 70$ km and $M_{totl}(0) = 40$ $M_\oplus$ to provide an illustrative case where the mass at the time of the LHB is 24 $M_\oplus$ and the final transition diameter is 87 km.

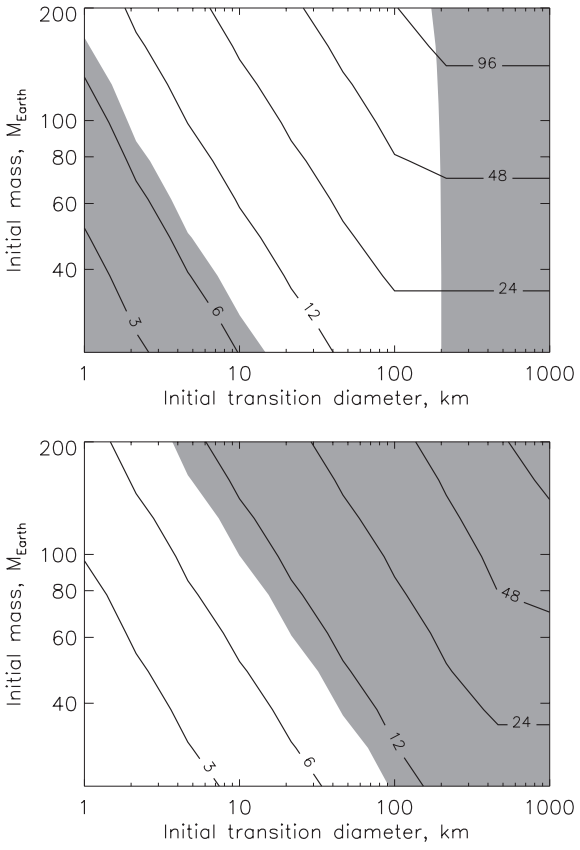

Figure 10. Dependence of mass at the time of the LHB on the initial conditions. Contours show the mass in Earth masses and the shaded regions represent runs that give a final transition diameter smaller or larger than the current constraints on the present day transition diameter. The runs shown in the top plot use the Löhne et al. (2008) $Q_D^\star$ and $q_p = 2.2$ and those in the bottom plot use the Leinhardt & Stewart (2009) $Q_D^\star$ and $q_p = 2.2$.

3.1.2 *Effect of a three-phase size distribution*

In Section 2, we used a size distribution with a slope defined by $q_d = 11/6$ to describe all of the objects. This results in a distribution where most of the mass is concentrated in the largest objects and so the collisional mass loss of the system was dependent on the collisional time-scale of the largest objects. We now find that the largest objects of size 2000 km now require a dispersal energy of $Q_D^\star(D_c) = 1.6 \times 10^7$ J kg^{-1} rather than the 200 J kg^{-1} used in Section 2. This now means the largest objects can only be destroyed by objects much larger than themselves and hence will never be destroyed in our simulations. Therefore, the largest KBOs in the Solar system are likely to be primordial as also found by the work of Farinella & Davis (1996). However, setting the slope of the primordial size distribution to 2.2 means that most of the mass is concentrated in objects with sizes $D \approx D_t$. As D_t increases, mass is still lost through collisions as the primordial planetesimals reach collisional equilibrium.

Fig. 11 shows how the spectral energy distribution (SED) changes when we use a three-phase size distribution. By comparing the lines for blackbody one phase and blackbody three phase, we can see that

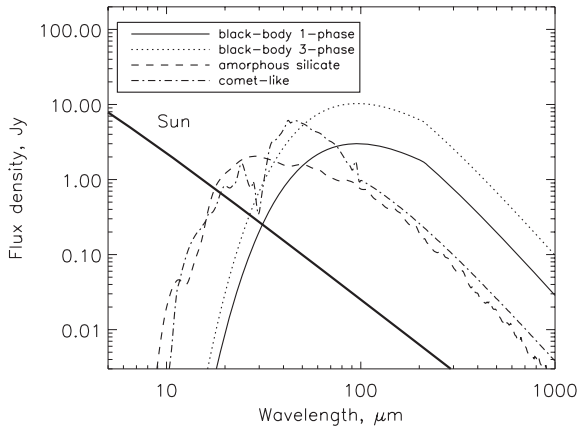

Figure 11. SED pre-LHB for blackbody grains with a single-slope size distribution and also blackbody grains, amorphous silicate grains and comet-like grains with the Löhne model of an evolving size distribution. The realistic grain models also include a three-phase size distribution and all of the three-phase models have an initial mass of 40 $M_\oplus$ and an initial transition diameter of 70 km.

the three-phase model increases the amount of flux emitted at all wavelengths, with a four-fold increase in the peak of the SED. Fig. 12 shows how the evolution of f, $F_\nu/F_{\nu\star}$ and $M_{\rm dust}$ changes when we use a three-phase size distribution. From this plot we can see that the increase in flux is present at all times. This increase in flux is due to the increase in the σ/M ratio. At early times, it is five times greater than that given in equation (2) and decreases to four times greater as $D_{\rm t}$ increases. This slight decrease can be seen in the dotted lines of Fig. 12 where the slope of the line becomes slightly steeper just prior to the LHB.

This result implies that before the LHB, the Solar system would have been amongst the brightest debris disc systems around Sun-like stars in 24 and 70 μm emission. Although plausible, this could be a result of our choice of parameters. For instance, in equation (18) we set $b_{\rm g} = 0.5$ giving us a power-law slope in the gravity regime of $q_{\rm g} = 5/3$, whereas recent observations suggest a value of $q_{\rm g} \approx 4/3$ might be more realistic (Fraser & Kavelaars 2009; Fuentes et al. 2009).

By changing from a single-slope power law to a three-phase power law and including a dispersal threshold that is dependent on size means that the Solar system's debris disc would have been significantly brighter, but the rest of the conclusions of Section 2 still hold. The 24 and 70 μm excesses still evolve in the same manner with a peak in the 24 μm excess still being seen at the time of the LHB. Both models also show that mass lost from collisions is likely to be important in the evolution of the Solar system's debris disc, although in the basic model the mass loss was from collisions of the largest objects whereas now we have shown that the mass loss is due to the evolution of the size distribution and the amount of mass lost is greatly dependent on the initial size distribution used.

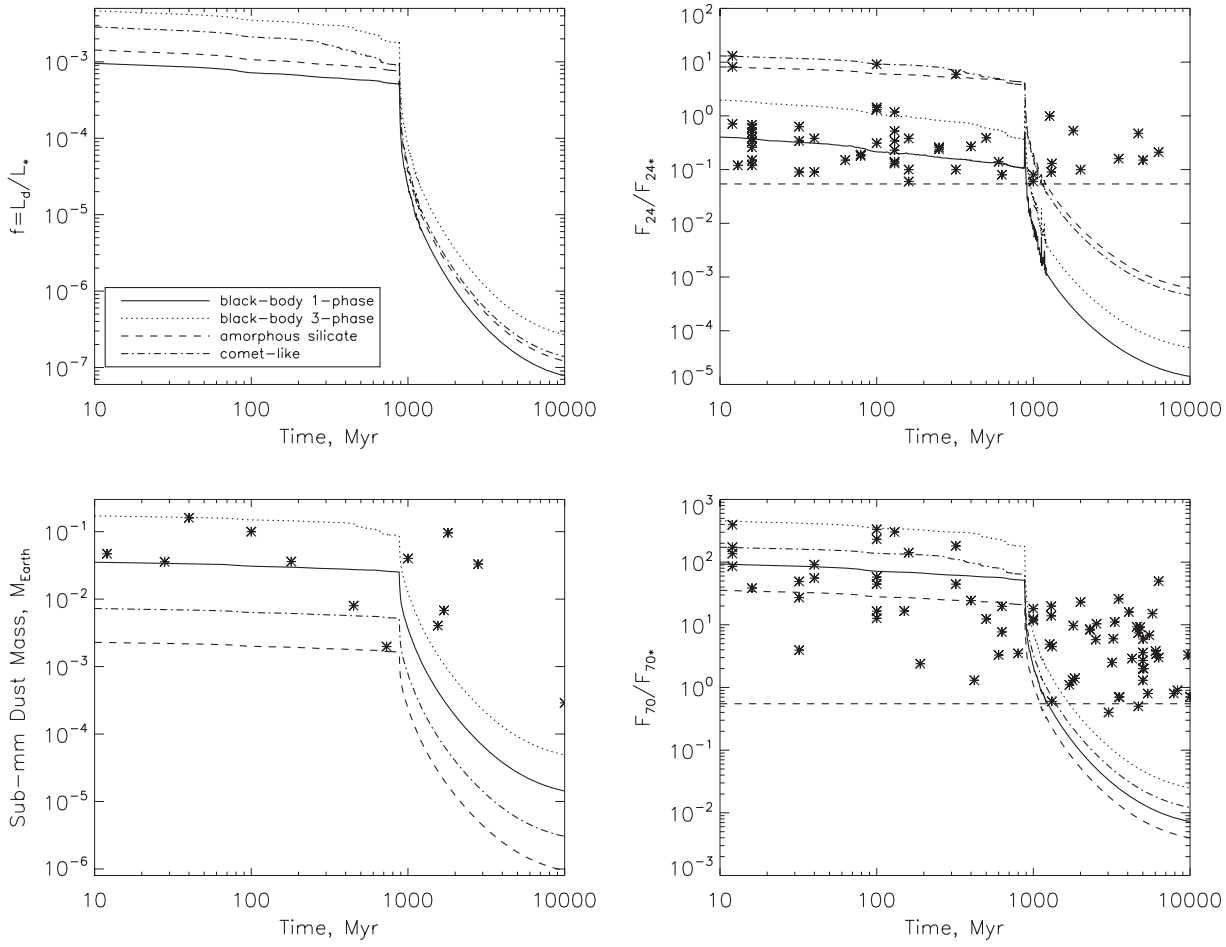

Figure 12. Same as Figs 4–6 but also including the blackbody three-phase size distribution model and the realistic grain models. The realistic grain models also include a three-phase size distribution and all of the three-phase models have an initial mass of 40 $M_\oplus$ and an initial transition diameter of 70 km.

3.2 SED model

In reality, particles do not emit or absorb efficiently at all wavelengths. Their emission and absorption efficiencies are dependent on their composition and porosity. Wyatt & Dent (2002) created a model that shows how the SED changes depending on the properties of the particles based on the compositional model of Li & Greenberg (1997). They used this model to find the most likely composition of the Fomalhaut debris disc. Here, we use this model to see how it changes the results of Section 2.

By relaxing the blackbody assumption, we change equations (3) and (4) so that

$$F_\nu = 2.35 \times 10^{-11} d^{-2} \sum_R \sum_D \sigma(R) Q_{\rm abs}(\lambda, D) \bar{\sigma}(D) \times B_\nu(\lambda, T(D, R)), \quad (27)$$

$$T(D, R) = (\langle Q_{\rm abs} \rangle_{T_\star} / \langle Q_{\rm abs} \rangle_{T(D,R)})^{1/4} T_{\rm bb}, \quad (28)$$

where $T_{\rm bb}$ is the blackbody temperature given by equation (4) and $Q_{\rm abs}$ (the absorption efficiency) is found using Mie theory, Rayleigh–Gans theory or geometric optics in the appropriate limits using optical properties from the compositional model.

To calculate the composition of the particles, the core-mantle model of Li & Greenberg (1997) is used. This assumes the particles to be formed of a silicate core surrounded by an organic refractory mantle where the silicate core makes up 1/3 of the total volume. The silicate material may be either amorphous or crystalline. The particles will have a given porosity (p) defining how much of the particles' volume is empty space, and a given fraction of water ($q_{\rm H_2O}$) defining how much of the empty space is filled by ice.

Although the composition of some of the largest KBOs has been inferred from spectroscopy (e.g. Barucci et al. 2008), it is the smaller grains (which have not been observed) that have a larger effect on the SED. In this paper, we will look at two extremes for the particle composition. The first grain composition replaces the blackbody grains by amorphous silicate grains with zero porosity and no ice. For this composition, $\rho = 2370$ kg m^{-3} and $D_{\rm bl} = 1.47\,\mu$m. For the second grain composition, we will assume that the grains have a similar composition to the 'comet-like' grains of Augereau et al. (1999). As such, this composition uses crystalline grains with $p = 0.93$ and $q_{\rm H_2O} = 0.38$. For this composition, $\rho = 590$ kg m^{-3} and $D_{\rm bl} = 0.85\,\mu$m.

3.2.1 *Effect of using a realistic grain model*

Fig. 11 shows how the SED for the realistic grain models compares to the blackbody models from Sections 2 and 3.1 (both realistic grain models also use the evolving size distribution described in Section 3.1). From this plot, we can see that by introducing realistic grains to the model, the peak of the SED clearly moves to a lower wavelength. This occurs because the majority of the emission is from particles in the size regime where they absorb radiation more efficiently than they emit it, which causes their temperature to increase more than if they were blackbodies (see equation 28). The SED also shows features in the emission due to the elements present in the grain, although these are much more prominent in the 'comet-like' model due to the presence of ice and the crystalline nature of the grains.

The fact that the peak of the wavelength emission has moved to a lower wavelength means that the 24 μm flux is much higher compared to the blackbody grains (see Fig. 12). So high that the Solar system would have been amongst the brightest discs at 24 μm before the LHB. This increase in 24 μm flux at young ages means that we no longer see the jump in $F_{24}/F_{24\star}$ that we saw for the blackbody grains at the time of the LHB. However, this jump is seen at lower wavelengths, such as those below 10 μm, as can be seen in Fig. 13 which shows the SED for the 'comet-like' grains before, during and after the LHB. The 70 μm flux is reduced when using realistic grain properties, although this is more pronounced for the amorphous silicate grains. This decrease is because the SED peak is at a lower wavelength and the total flux has decreased due to the decrease in emitting efficiency of the particles.

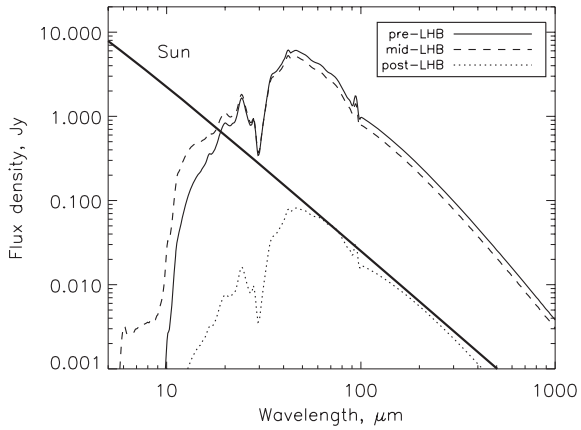

Figure 13. Same as Fig. 3 but for the comet grain model.

Using realistic grain models changes the density from that assumed previously, especially when porous grains are used. The lower density of the 'comet-like' grains has the effect of increasing the σ/M ratio which reduces the collisional lifetime of all particles. This reduction in collisional lifetime means that a greater final transition diameter is reached. For the case of the 'comet-like' grains, a final transition diameter of 117 km is reached. However, it should be noted that we have assumed objects of all sizes to have the same density and porosity, whereas the large KBOs have lower porosities and so higher densities – Varuna, for example, is estimated to have a porosity of 0.05–0.3 (Jewitt & Sheppard 2002) – and therefore there would not be as much collisional evolution as we have suggested here. If amorphous silicate properties are used, the density of the planetesimals is much higher and so they do not collisionally evolve and the transition diameter does not change.

The high water–ice content of the 'comet-like' model means that these particles are likely to undergo ice sublimation close to the Sun, however, the precise effects of sublimation on the size distribution are unknown. Since particles would only come close enough to the Sun for a brief period during the LHB (see Fig. 1), we would only expect ice sublimation to affect our results during the brief mid-LHB phase and we intend to explore this effect in a future work.

Introducing realistic grains to our model has the effect of moving the SED to shorter wavelengths, thus increasing the mid-IR flux emitted. The same effect could be approximated with blackbody grains if they were assumed to be much closer to the star and therefore have a greater temperature.

Of the four models presented in this paper, the 'comet-like' is the most realistic. This predicts that the current fractional luminosity is 3×10^{-7} and the current submillimetre dust mass is 7×10^{-6} M$_\oplus$. Both of which are within the observational limits (see Sections 2.3 and 2.4).

4 CONCLUSIONS

In this paper, we present a new look at the history of the Solar system. Starting with the Nice model for the evolution of the Solar system, we demonstrate how the evolving spatial distribution of planetesimals in the system changes the thermal emission of dust produced in planetesimal collisions. We started with a simple model that used a single-phase power law to convert between mass of planetesimals and surface area and assumed blackbody emission (see Section 2). We find that this model predicts that the primordial Kuiper belt would have been detectable at 24 and 70 μm before the LHB. During the LHB, more hot dust would have been produced as many of the KBOs are scattered inwards towards the Sun causing a peak in the 24 μm emission. Within a few hundred million years of the LHB, the dynamical depletion of the Kuiper belt renders it undetectable at 24 and 70 μm.

Statistics from surveys of Sun-like stars (e.g. Trilling et al. 2008) show that the number of stars with an observable excess at 24 μm decreases with stellar age and the number of stars with an observable excess at 70 μm remains approximately constant with stellar age. An LHB-like event causes a drop in excess ratio of approximately 4 orders of magnitude at both these wavelengths (see Fig. 12) showing that such major clearing events must be rare and that most debris discs that are detectable just after 10 Myr lose mass through collisions rather than through dynamical instabilities. This allows us to set an upper limit of 12 per cent on the fraction of Sun-like stars that go through an LHB.

Fig. 5 shows that the period of increased 24 μm emission only lasts for ∼15 Myr. If we assume that the average age of Sun-like stars that we observe is 5 Gyr then there is at most a 0.04 per cent chance of observing a star going through an LHB. However, the bombardment from the asteroids lasts about five times longer (Gomes et al. 2005) and so could increase this possibility to 0.2 per cent. Therefore, of the 26 Sun-like field stars older than 10 Myr found to have a 24 μm excess out of a compiled sample of 413 (see table 5 in Gáspár et al. 2009), approximately one could be an observation of a current LHB event. Certain systems such as η Corvi which have both hot and cold dust but too much hot dust to be explained by collisional evolution alone (Wyatt et al. 2007a) may still be explained by an LHB-like event.

Although in this model we have just considered the evolution of the Solar system as described by the Nice model, this paper gives enough detail for this simple model to easily be applied to the output of any numerical simulation of planetesimals to give an indication of its observable properties.

In Section 3, we removed the major assumptions of the initial model by including a three-phase power-law size distribution that depends on collisional history. Changing the size distribution has the effect of greatly increasing the flux emitted. Having a size distribution that changes during the simulation also means that mass is also lost due to collisions. For instance, if we start with an initial transition diameter of 70 km, an initial mass of 40 $M_\oplus$ is required to leave us with the 24 $M_\oplus$ at the time of the LHB that is necessary for the LHB to take place. However, this assumes that the KBOs are as strong as the Benz & Asphaug (1999) case. If they are as weak as Leinhardt & Stewart (2009) suggest (and our simplistic combination of collisional and dynamical mass loss is correct) then this shows that the Nice model cannot be used to explain the LHB since either too much mass is lost through collisional grinding or the final transition diameter is unrealistic. The Nice model description of the migration of the planets is not ruled out by this, only the need for there to be a delay before the 2:1 MMR crossing of Jupiter and Saturn.

We also find that changing the grain properties to resemble more realistic grains has the effect that the spike in 24 μm emission is no longer seen as the peak wavelength is shorter and so the 24 μm emission is initially much higher. However, peaks in emission at lower wavelengths such as 10 μm would still be possible indicators of an LHB-like transient event. The wavelengths the spike appears at also depend on the heliocentric distance of the disc. If the disc starts further out in the system, then it could still give a spike in the 24 μm emission.

One major caveat of this work is that we have only concentrated on the emission from the Kuiper belt. Since this is far from the Sun, most of the emission will be from cold dust and thus we are underestimating the warm emission and, therefore, the 24 μm flux. In future work, we intend to include the asteroid belt in this model and investigate the effect of sublimation from comets.

ACKNOWLEDGMENTS

We would like to thank Zoë Leinhardt for explaining the limitations of the standard dispersal threshold model and for her comments on the paper. We also thank an anonymous reviewer for useful comments and suggestions, which have helped to improve this paper. MB acknowledges the UK PPARC/STFC for a research studentship.

REFERENCES

Augereau J. C., Lagrange A. M., Mouillet D., Papaloizou J. C. B., Grorod P. A., 1999, A&A, 348, 557
Backman D. E., Dasgupta A., Stencel R. E., 1995, ApJ, 450, L35
Barucci M. A., Brown M. E., Emery J. P., Merlin F., 2008, Composition and Surface Properties of Transneptunian Objects and Centaurs. The Solar System Beyond Neptune, Univ. Arizona Press, Tuscon, p. 143
Beichman C. A. et al., 2006, ApJ, 652, 1674
Benz W., Asphaug E., 1999, Icarus, 142, 5
Bernstein G. M., Trilling D. E., Allen R. L., Brown M. E., Holman M., Malhotra R., 2004, AJ, 128, 1364
Bottke W. F., Durda D. D., Nesvorný D., Jedicke R., Morbidelli A., Vokrouhlický D., Levison H., 2005, Icarus, 175, 111
Campo Bagatin A., Farinella P., Petit J.-M., 1994, Planet Space Sci., 42, 1099
Carpenter J. M. et al., 2009, ApJS, 181, 197
Chiang E., Lithwick Y., Murray-Clay R., Buie M., Grundy W., Holman M., 2007, in Reipurth B., Jewitt D., Keil K., eds, Protostars and Planets V. A Brief History of Transneptunian Space. Univ. Arizona Press, Tuscon, p. 895
Dohnanyi J. S., 1968, in Kresak L., Millman P. M., eds, IAU Symp. 33, Physics and Dynamics of Meteors. Reidel, Dordrecht, p. 486
Farinella P., Davis D. R., 1996, Sci, 273, 938
Farinella P., Paolicchi P., Zappala V., 1982, Icarus, 52, 409
Fraser W. C., Kavelaars J. J., 2009, AJ, 137, 72
Fuentes C. I., Holman M. J., 2008, AJ, 136, 83
Fuentes C. I., George M. R., Holman M. J., 2009, ApJ, 696, 91
Gáspár A., Rieke G. H., Su K. Y. L., Balog Z., Trilling D., Muzzerole J., Apai D., Kelly B. C., 2009, ApJ, 697, 1578
Gladman B., Kavelaars J. J., Petit J.-M., Morbidelli A., Holman M. J., Loredo T., 2001, AJ, 122, 1051
Gomes R. S., 1997, AJ, 114, 396
Gomes R., Levison H. F., Tsiganis K., Morbidelli A., 2005, Nat, 435, 466
Gomes R. S., Fernández J. A., Gallardo T., Brunini A., 2008, The Scattered Disk: Origins, Dynamics, and End States. The Solar System Beyond Neptune. Univ. Arizona Press, Tuscon, p. 259
Greaves J. S., Holland W. S., Jayawardhana R., Wyatt M. C., Dent W. R. F., 2004a, MNRAS, 348, 1097
Greaves J. S., Wyatt M. C., Holland W. S., Dent W. R. F., 2004b, MNRAS, 351, L54
Greaves J. S. et al., 2005, ApJ, 619, L187

Greaves J. S., Wyatt M. C., Bryden G., 2009, MNRAS, 397, 757
Gustafson B. A. S., 1994, Annu. Rev. Earth Planet. Sci., 22, 553
Habing H. J. et al., 2001, A&A, 365, 545
Hillenbrand L. A. et al., 2008, ApJ, 677, 630
Housen K. R., Holsapple K. A., 1990, Icarus, 84, 226
Jewitt D. C., Sheppard S. S., 2002, AJ, 123, 2110
Jorgensen U. G., 1991, A&A, 246, 118
Kenyon S. J., Luu J. X., 1999, AJ, 118, 1101
Kring D. A., Cohen B. A., 2002, J. Geophys. Res., 107, 5009
Krivov A. V., Sremčević M., Spahn F., 2005, Icarus, 174, 105
Leinhardt Z. M., Stewart S. T., 2009, Icarus, 199, 542
Levison H. F., Terrell D., Wiegert P. A., Dones L., Duncan M. J., 2006, Icarus, 182, 161
Levison H. F., Morbidelli A., Vanlaerhoven C., Gomes R., Tsiganis K., 2008a, Icarus, 196, 258
Levison H. F., Morbidelli A., Vokrouhlický D., Bottke W. F., 2008b, AJ, 136, 1079
Li A., Greenberg J. M., 1997, A&A, 323, 566
Löhne T., Krivov A. V., Rodmann J., 2008, ApJ, 673, 1123
Marcy G., Butler R. P., Fischer D., Vogt S., Wright J. T., Tinney C. G., Jones H. R. A., 2005, Prog. Theor. Phys. Suppl., 158, 24
Minato T., Köhler M., Kimura H., Mann I., Yamamoto T., 2006, A&A, 452, 701
Moór A., Ábrahám P., Derekas A., Kiss C., Kiss L. L., Apai D., Grady C., Henning T., 2006, ApJ, 644, 525
Morbidelli A., Levison H. F., Tsiganis K., Gomes R., 2005, Nat, 435, 462
Moro-Martín A. et al., 2007, ApJ, 668, 1165
Moro-Martín A., Wyatt M. C., Malhotra R., Trilling D. E., 2008, Extrasolar Kuiper Belt Dust Disks. The Solar System Beyond Neptune, Univ. Arizona Press, Tuscon, p. 465
Najita J., Williams J. P., 2005, ApJ, 635, 625
O'Brien D. P., Greenberg R., 2003, Icarus, 164, 334
Petit J.-M., Farinella P., 1993, Celest. Mech. Dyn. Astron., 57, 1
Petit J.-M., Kavelaars J., Gladman B., Loredo T., 2008, Size Distribution of Multikilometer Transneptunian Objects. The Solar System Beyond Neptune, Univ. Arizona Press, Tuscon, p. 71
Plavchan P., Jura M., Lipscy S. J., 2005, ApJ, 631, 1161
Sackmann I.-J., Boothroyd A. I., 2003, ApJ, 583, 1024
Sheret I., Dent W. R. F., Wyatt M. C., 2004, MNRAS, 348, 1282
Stern S. A., 1996a, AJ, 112, 1203
Stern S. A., 1996b, A&A, 310, 999
Stewart S. T., Leinhardt Z. M., 2009, ApJ, 691, L133
Strom R. G., Malhotra R., Ito T., Yoshida F., Kring D. A., 2005, Sci, 309, 1847
Tera F., Papanastassiou D. A., Wasserburg G. J., 1974, Earth Planet. Sci. Lett., 22, 1
Trilling D. E. et al., 2007, ApJ, 658, 1289
Trilling D. E. et al., 2008, ApJ, 674, 1086
Tsiganis K., Gomes R., Morbidelli A., Levison H. F., 2005, Nat, 435, 459
Williams J. P., Andrews S. M., 2006, ApJ, 653, 1480
Wood B. E., Müller H.-R., Zank G. P., Linsky J. L., Redfield S., 2005, ApJ, 628, L143
Wyatt M. C., 2005, A&A, 433, 1007
Wyatt M. C., 2008, ARA&A, 46, 339
Wyatt M. C., Dent W. R. F., 2002, MNRAS, 334, 589
Wyatt M. C., Dermott S. F., Telesco C. M., Fisher R. S., Grogan K., Holmes E. K., Piña R. K., 1999, ApJ, 527, 918
Wyatt M. C., Dent W. R. F., Greaves J. S., 2003, MNRAS, 342, 876
Wyatt M. C., Greaves J. S., Dent W. R. F., Coulson I. M., 2005, ApJ, 620, 492
Wyatt M. C., Smith R., Greaves J. S., Beichman C. A., Bryden G., Lisse C. M., 2007a, ApJ, 658, 569
Wyatt M. C., Smith R., Su K. Y. L., Rieke G. H., Greaves J. S., Beichman C. A., Bryden G., 2007b, ApJ, 663, 365
Wyatt M. C., Booth M., Payne M. J., Churcher L. J., 2009, MNRAS, submitted
Zuckerman B., 2001, ARA&A, 39, 549

This paper has been typeset from a TEX/LATEX file prepared by the author.